CMS Physics Analysis Summary

Contact: cms-pag-conveners-ewk@cern.ch 2012/03/12

Study of the dijet invariant mass distribution in W$\to \ell\nu$ plus jets events produced in pp collisions at $\sqrt{s} = 7$ TeV

The CMS Collaboration

Abstract

The invariant mass spectrum of the two jets with the highest transverse momenta in events with two or three jets, produced in association with a W boson, is presented. The analyzed data sample corresponds to an integrated luminosity of 4.7 fb^{-1} collected with the CMS detector at $\sqrt{s} = 7$ TeV. The observed dijet mass distribution is modeled empirically with a set of templates obtained from simulated event samples. We set an upper limit of 1.3 pb at 95% confidence level on the production cross section times W$\to \ell\nu$ branching fraction for a generic Gaussian signal peaked at 150 GeV. Several theoretical models that predict a resonant enhancement near 150 GeV are excluded.

1 Introduction

This document presents the study of the invariant mass spectrum m_{jj} of the two jets with the highest transverse momentum (p_{T}) in events with two or three jets produced in association with a W boson. In events containing a lepton plus jets, the CDF collaboration reported evidence [1] for an excess over the m_{jj} distribution expected from the standard model (SM) processes. The DØ collaboration carried out a similar analysis, but could not confirm this result [2].

We search for anomalous dijet production in the data sample with an integrated luminosity of 4.7 fb^{-1}, collected by the CMS experiment in 2010 and 2011 at $\sqrt{s} = 7$ TeV. Events are selected with one well identified and isolated lepton, large missing transverse energy, and two or three high p_{T} jets. The selection criteria are similar to those used at the Tevatron, with modifications to account for higher background rates at the LHC and different experimental conditions. The observed m_{jj} distribution is modeled by means of a fit to a set of template shapes obtained from simulated event samples in the region between 40 GeV and 400 GeV.

We investigate the presence of a possible resonant enhancement in the dijet mass spectrum near 150 GeV for three representative models. These are production of a technicolor π_T from the decay of a technicolor ρ_T [3, 4], of a leptophobic $\mathrm{Z}' \to jj$ [5, 6], and of the SM Higgs boson. In all three hypotheses, the new particle is produced in association with a W boson, and decays into a pair of jets. Furthermore, we consider a generic Gaussian signal model obtained from a delta function at $m_{jj} = 150$ GeV convolved with a detector resolution of $\sigma_{m_{jj}} \sim 15$ GeV.

2 CMS detector

The CMS coordinate system has its origin at the centre of the detector, with the z-axis pointing along the direction of the counterclockwise beam. The azimuthal angle is denoted as ϕ, the polar angle as θ, and the pseudorapidity is defined as $\eta = -\ln[\tan(\theta/2)]$. The central feature of the CMS detector is a superconducting solenoid, of 6 m internal diameter, that produces an axial magnetic field of 3.8 T. Located within the field volume there are the silicon pixel and strip tracker extending up to $|\eta| = 2.5$, a lead-tungstate crystal electromagnetic calorimeter (ECAL) and a brass/scintillator hadronic calorimeter, both extending up to $|\eta| = 3$. Outside the field volume, in the forward region ($3 < |\eta| < 5$), is an iron/quartz-fiber hadronic calorimeter. Muons are measured in gas detectors embedded in the steel return yoke outside the solenoid, in the pseudorapidity range $|\eta| < 2.4$. A detailed description of the CMS experiment can be found in Ref. [7].

3 Event reconstruction and selection

Jets and missing transverse energy, $\not\!\!E_{\mathrm{T}}$ [8, 9], are reconstructed from the object collection obtained with the particle flow algorithm [10] which combines information from several subdetectors. Jets are formed with the anti-k_T clustering algorithm [11] with the size parameter $\Delta R = 0.5$. We require $|\eta| < 2.4$ for jets in order for them to be within the tracker acceptance. Charged particles with tracks not originating at the primary vertex are not considered for jet clustering [12, 13]. The azimuthal separation, $\Delta\phi_{\not\!\!E_{\mathrm{T}},\text{lead jet}}$, between the leading jet and the $\not\!\!E_{\mathrm{T}}$ direction should be larger than 0.4 to reduce mismeasured $\not\!\!E_{\mathrm{T}}$. Jets are required to satisfy identification criteria that eliminate jets originating from noisy channels in the hadron calorimeter [14]. Jet energy corrections (JEC) [15] are applied to account for the jet energy response as a function of η and p_{T}, and to correct for contribution from additional proton-proton interactions, *i.e.*, event pile-up. The jet p_T resolution varies from 15% at $p_T = 40$ GeV to 6% at $p_T =$

Table 1: Summary of selection criteria.

$W \to \ell\nu$ selection	Jet selection
Single lepton trigger	$p_T^{\text{lead jet}} > 40$ GeV
High-quality lepton ID and isolation	$p_T^{\text{2nd jet}} > 30$ GeV
Muon (electron) $p_T > 25(35)$ GeV	dijet $p_T > 45$ GeV
$\not{E}_T > 25(30)$ GeV for muon (electron) samples	$\Delta\eta_{jj} \leq 1.2$
W transverse mass > 50 GeV	$\Delta\phi(\not{E}_T, \text{lead jet}) > 0.4$
Second lepton veto	$0.3 < p_T^{\text{2nd jet}}/m_{jj} < 0.7$

400 GeV. The dijet mass, m_{jj} is calculated from the corrected four-momentum vectors of the two highest p_T jets.

Electrons are identified as clusters of ECAL energy deposits matched to tracks from the silicon tracker within the ECAL fiducial volume with $|\eta| < 2.5$, with exclusion of the region $1.44 < |\eta| < 1.57$ where services and cables exit. Muons candidates are reconstructed in the fiducial region $|\eta| < 2.1$ by combining information from the silicon tracker and from the muon chambers by means of a global fit. Electron and muon candidates need to fulfill quality criteria standards established by the measurement of the inclusive W and Z cross sections [9]. In addition, all leptons have to be well separated from hadronic activity in the event. Jets which fall within a radius 0.3 around a lepton candidate in the $\eta - \phi$ plane are disregarded.

The data used in this analysis passed a suite of single lepton triggers. The majority of the data was collected with trigger transverse momentum thresholds of 24 GeV for muons and 25–32 GeV for electrons. We devise selection criteria similar to those used at the Tevatron [1, 2]. A more stringent requirement for the jet topology in the event is applied, as suggested in [16] to reduce the W plus jets contribution. Compared to the Tevatron, at the LHC this contribution is about one order of magnitude larger.

We select events containing a good quality, isolated muon (electron) with $p_T > 25$ (35) GeV and $\not{E}_T > 25$ (30) GeV. The muon (electron) selection efficiency is about 95% (64%), while the trigger efficiency for the selected muons (electrons) is about 94% (90%). The transverse mass M_T of the W candidate is defined as $M_T \equiv \sqrt{2\, p_T^l\, \not{E}_T\, (1 - \cos(\phi_l - \phi_{\not{E}_T}))}$, where ϕ_l and $\phi_{\not{E}_T}$ are the azimuthal angles of the lepton and $\not{E}_T$, respectively. The transverse mass M_T has to be larger than 50 GeV to select a rather pure sample of W boson events. Events with a second lepton passing looser quality criteria and with $p_T^\mu > 10$ GeV or $p_T^e > 20$ GeV are disregarded to reduce the Drell-Yan contribution. Furthermore, we require the presence of exactly two or three jets in the event with $p_T > 40$ GeV for the leading p_T jet and $p_T > 30$ GeV for the second and third jets. The selected jets and the lepton from the W decay are required to originate from the same primary vertex. The opening angle between the two leading jets needs to satisfy $|\Delta\eta_{jj}| < 1.2$ and the transverse momentum of the dijet system needs to be $p_T^{jj} > 45$ GeV. We require $0.3 < p_T^{\text{2nd jet}}/m_{jj} < 0.7$ in order to take into account that the distribution of the ratio of the second leading jet p_T and m_{jj} has a more pronounced shape for WW or new hypothetical physics resonances [16]. Table 1 provides a summary of the selection requirements.

4 Data and simulated event samples

The selected data sample is dominated by events with W plus two or more jets. Smaller contributions come from top pair ($t\bar{t} \to \ell\nu jj$), single top ($pp \to tq \to \ell\nu jj$), Drell-Yan plus two or more jets, and multijet production. A small fraction of events is due to WW and WZ diboson production with one W decaying leptonically and another W or Z decaying hadronically. Large samples of simulated events of various SM processes are used to model the shape of their m_{jj} distributions.

A reference sample of W boson events is generated with the MADGRAPH [17] event generator, interfaced to the PYTHIA [18] program for parton shower simulation. The MADGRAPH generator produces parton-level events with a vector boson and up to four partons on the basis of a matrix-element calculation. The matching scale is $\mu^2 = 20$ GeV and the factorization and renormalization scales are set at $q^2 = M^2_{W/Z} + p^2_{T,W/Z}$. Four additional samples of W events are generated and are also used in the modeling of the W plus jets distribution. In these alternative samples, the scales are increased and reduced by a factor of two with respect to those of the reference sample. Samples of $t\bar{t}$ and Drell-Yan events are also generated with MADGRAPH, with the same matching and factorization/renormalization scales as for the reference W sample. Single top production is modeled with POWHEG [19] interfaced to PYTHIA. Multijet and diboson samples (WW, WZ, ZZ) are generated with PYTHIA. The PYTHIA parameters for the underlying event modeling are set to the Z2 tune [20]. The set of parton distribution functions used is CTEQ6LL [21]. Simulated event samples of a possible new physics signal from the technicolor or the WH models are generated with PYTHIA, while the sample of leptophopic Z′ production is generated with MADGRAPH interfaced to PYTHIA. All samples are then simulated using a GEANT4-based model [22] of the CMS detector, multiple proton-proton interactions are taken into account and the triggers are emulated. Finally all simulated events are reconstructed and analyzed with the same software as used to process collision data and are corrected for any difference in the performance of the trigger, lepton reconstruction, and $\not\!\!E_T$ resolution.

5 Fit to the dijet invariant mass distribution

We determine the relative contribution of the known SM processes to the observed m_{jj} spectrum using an unbinned maximum likelihood fit in the range between 40 GeV and 400 GeV. The fit is performed separately for the electron and muon channels and for the 2 jets and 3 jets samples since relative background contributions and composition differ. The m_{jj} region [123, 186] GeV, which corresponds to about a $\pm 2\sigma$ window within the binning used to model the m_{jj} shape, is excluded from this fit in order to arrive at an unbiased estimate of a possible resonant enhancement in this region.

Table 2 lists the SM processes included in the fit. The normalization of the dominant W plus jets contribution is a free fit parameter. The normalization of all other event classes is allowed to vary within a Gaussian constraint around the central values. For multijet events, this central value is obtained from a separate fit to the $\not\!\!E_T$ distribution [9] and the Gaussian constraint is driven by the corresponding fit error estimate. The central value for all other processes is obtained from next-to-leading order (NLO) or next-to-NLO (NNLO) calculations and the Gaussian constraint reflects the theoretical uncertainties. With the exception of multijet production, the m_{jj} template distribution shapes for all processes are obtained from simulated event samples. Multijet events contribute when jets are misidentified as isolated leptons. Hence their m_{jj} shape can be derived from data events with lepton candidates that fail the isolation requirement (muon case) or that fail the strict electron quality and isolation reqirements but pass

Table 2: Determination of the m_{jj} shape and normalization. External constraints are assumed Gaussian.

Process	Shape	External constraint on normalization
W plus jets	MC/data	Unconstrained
Diboson	MC	Constrained: (NLO) 61.2 pb $\pm$ 10% [23]
$t\bar{t}$	MC	Constrained: (NLO) 163 pb $\pm$ 7% [24]
Single top	MC	Constrained: (NNLO) [25–27] $\pm$ 5%
Drell-Yan plus jets	MC	Constrained: (NLO, $m_{ll} > 50$ GeV) 3048 pb $\pm$ 4.3% [23]
Multijet	data	Constrained: $\not\!\!E_T$ fit in data $\pm$ 50% (100%) for electron (muon)

less strict ones.

The description of the observed m_{jj} spectrum using the template derived from the reference MADGRAPH sample for the dominant W plus jets component is not adequate. No significant improvement is observed with any of the alternative samples. Hence the m_{jj} template for the W plus jets component is modeled as a combination of three shapes:

$$\mathcal{F}_{\text{W+jets}} = \alpha \cdot \mathcal{F}_{\text{W+jets}}(\mu_0^2, q'^2) + \beta \cdot \mathcal{F}_{\text{W+jets}}(\mu'^2, q_0^2) + (1 - \alpha - \beta) \cdot \mathcal{F}_{\text{W+jets}}(\mu_0^2, q_0^2), \qquad (1)$$

where $\mathcal{F}_{\text{W+jets}}$ denotes the m_{jj} shape of the MADGRAPH sample in question, normalized to unity. The parameters μ_0 (μ') and q_0 (q') correspond to the default (alternative) values of μ and q respectively, and α and β are relative fractions allowed to vary in the fit. We take $\mu' = 2\mu_0$, if $\mu > \mu_0$ and $\mu' = 0.5\mu_0$, if $\mu < \mu_0$; similarly, $q' = 2q_0$, if $q > q_0$ and $q' = 0.5q_0$, if $q < q_0$. Since the fit determines α and β simultaneously with the relative contributions of the SM components, the final fit result takes the uncertainty of α and β and hence the shape uncertainty of the m_{jj} distribution for W plus jets properly into account.

Table 3: Event yields determined from a likelihood fit to the data. The total uncertainty includes the effect of correlation among the individual contributions using the full covariance matrix.

Process	Muon channel		Electron channel	
	2 jets	3 jets	2 jets	3 jets
W plus jets	59430$\pm$519	13419$\pm$360	29989$\pm$1202	8600$\pm$287
Dibosons	1167$\pm$108	314$\pm$31	646$\pm$61	174$\pm$17
$t\bar{t}$	4258$\pm$290	8753$\pm$371	2413$\pm$164	4085$\pm$242
Single top	1663$\pm$82	945$\pm$47	864$\pm$43	492$\pm$25
Drell-Yan plus jets	1731$\pm$74	528$\pm$23	1000$\pm$43	343$\pm$15
Multijet	28$\pm$284	0 $\pm$ 90	4024$\pm$1181	330$\pm$160
Fit χ^2 probability	0.439	0.605	0.966	0.988
Total from fit	68277$\pm$307	23960$\pm$192	38935$\pm$228	14024$\pm$142
Data	67900	24046	38973	14145
In the test region 123 GeV $< m_{jj} <$ 186 GeV excluded from the fit				
Total	14494$\pm$125	7693$\pm$95	7925$\pm$92	4319$\pm$70
Data	14050	7751	8023	4438

Figure 1a shows the observed m_{jj} distribution for all four channels combined, together with the contribution of various SM processes whose normalizations are obtained from the fit. Figure 1b shows the same distribution after subtracting all SM contributions from data except for

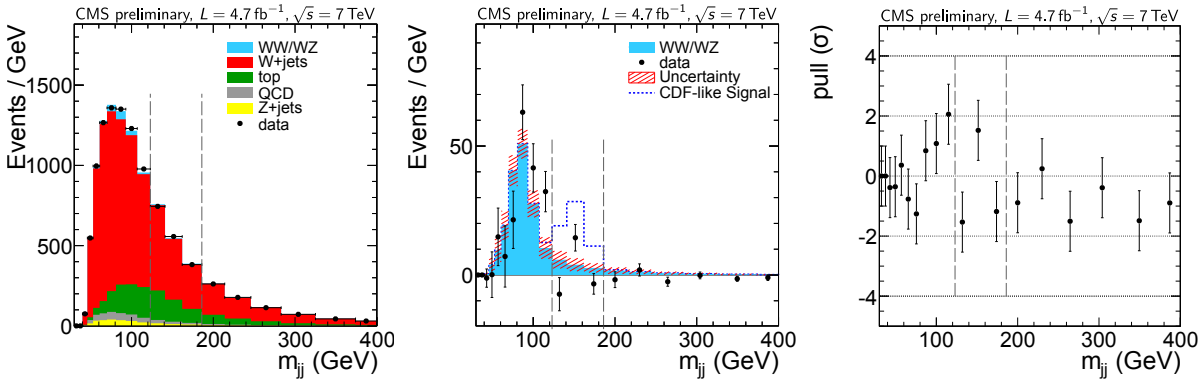

(a) (b) (c)

Figure 1: (a) Distribution of the invariant mass spectrum of the leading two jets observed in data including all four categories combined (muon plus 2 jets, muon plus 3 jets, electron plus 2 jets, and electron plus 3 jets). Overlaid are the template distributions used in the likelihood fit to the measured m_{jj} distibution, with their relative normalization as obtained in the fit. The region between the vertical dotted lines is excluded in the fit. Depicted is the number of events per GeV, *i.e.*, the raw event count can be obtained by multiplying with the bin width. (b) The same distribution after subtraction of all SM components except the electroweak diboson WW/WZ. Error bars correspond to the statistical uncertainty. The band represents the systematic uncertainty in the sum of the SM components. (c) The normalized residual: [data - fit] / fit uncertainty.

electroweak diboson WW/WZ events. Except for a peak near 80 GeV from diboson events no other peak is visible in the entire spectrum. Figure 1c shows the normalized residual, *i.e.*, pull distribution defined as [data - fit]/ fit uncertainty, where the uncertainty is the combined statistical and systematic one. Table 3 presents the yields of various SM components obtained from the fit. The sum of all the contributions is compared with the number of observed data events. All numbers but those in the last two rows are for the m_{jj} range [40, 400] GeV. The last two rows compare the observed and fitted contributions in the m_{jj} range [123, 186] GeV that is excluded in the fit. The data agree with the SM expectation throughout, and we find no significant excess in the test region.

6 Fit validation and systematic error estimate

We validate the fit procedure by performing pseudo-experiments. In each experiment, we generate the m_{jj} distribution of the SM processes of the sample size observed in data, taking into account the correlation among the yields. We then repeat the fit on each sample. The resulting yields and pull distributions indicate that the bias on the total yield is below 0.2% and that the fit understimates the yield uncertainty slightly. These effects are corrected for in the final result. Uncertainties in the jet energy scale (JES) are estimated in a sample of W bosons decaying hadronically in a highly pure sample of semileptonic $\mathrm{t\bar{t}}$ events. The mean and resolution of the reconstructed dijet (*i.e.*, W) mass distribution in data agree within 0.6% with the expectation from simulation, for the same level of the statistical accuracy as the measurement. This good agreement is further confirmed by including an additional free parameter in the fit to allow for shifts of the JES between data and simulation. A small difference in $\not\!\!E_{\mathrm{T}}$ resolution [8] between data and simulation affects the signal acceptance for the new physics models under consideration at the 0.5% level. Further systematic uncertainties are due to the uncertainty of the trigger efficiency estimates in data, which is 1%, and the estimate of lepton reconstruction

and selection efficiency, which is 2% [9]. The uncertainty in the luminosity determination is 4.5% [28].

7 Results on presence of possible resonant enhancement

We investigate the presence of a possible resonant enhancement in the dijet mass spectrum near 150 GeV for the technicolor, the leptophobic Z′, the WH, and a generic Gaussian signal model obtained from a delta function at $m_{jj} = 150$ GeV convolved with the CMS detector resolution of 15 GeV. The number of expected signal events N^{Signal} at the LHC for a given cross section at the Tevatron can be determined by considering the ratio of the predicted cross sections for our reference process, that is, WH production with $M_H = 150$ GeV. This process is dominated by quark-antiquark ($q\bar{q}$) annihilation. Since $q\bar{q}$ processes have the smallest increase in partonic luminosity from Tevatron to LHC, this choice provides a conservative limit.

$$\sigma^{dijet-resonance}_{\rm LHC} = \sigma^{dijet-resonance}_{\rm Tevatron} \times \frac{\sigma^{WH}_{\rm LHC}}{\sigma^{WH}_{\rm Tevatron}}, \quad (2)$$

$$N^{Signal} = \sigma^{dijet-resonance}_{\rm LHC} \times BR(W \to \ell\nu) \times (\varepsilon \times \mathcal{A}) \times \int \mathcal{L}{\rm dt}, \quad (3)$$

where $\sigma^{WH}_{\rm LHC} = 46.8$ fb [29] and $\sigma^{WH}_{\rm Tevatron} = 12$ fb [30] are the theory cross sections for WH production at the LHC and the Tevatron, respectively, $\varepsilon \times \mathcal{A}$ denotes efficiency $\times$ acceptance for WH events, BR stands for branching fraction [31], and $\int \mathcal{L}{\rm dt}$ is the integrated luminosity. The values of cross section and $\varepsilon \times \mathcal{A}$ for these models are given in Table 4. A generic Gaussian signal normalized to $\sigma_{\rm Tevatron} = 4$ pb corresponds to $\sigma_{\rm LHC} \times BR(W \to \ell\nu) = 3.4$ pb.

Signal Model	$\sigma \times BR$ (pb)	$\varepsilon \times \mathcal{A}$			
		electron 2 jets	electron 3 jets	muon 2 jets	muon 3 jets
WH	0.0145	0.038	0.013	0.060	0.019
Technicolor [3, 4]	1.58	0.039	0.011	0.065	0.020
Z' [5, 6]	1.72	0.042	0.014	0.070	0.023

Table 4: The cross section times W$\to \ell\nu$ branching ratio for various signal models and their overall reconstruction efficiency.

Since we observe no resonant enhancement, we proceed to set exclusion limits using a modified frequentist CL_S [31, 32] with profile likelihood as the test statistic. Inputs to the limit setting procedure are the m_{jj} distribution obtained by combining the SM components from the fit, the observed distribution in data, and the expectation from the dijet resonance model under consideration.

Figure 2a shows the distributions of observed and expected CL_S values for a generic Gaussian signal after combining the results of all four event categories. We set an upper limit of 1.3 pb at 95% confidence level (CL) on the production cross section $\times BR(W \to \ell\nu)$. Upper limits on cross section computed at 95% CL for the technicolor, the leptophobic Z′, and the WH ($M_H =$ 150 GeV) signal models are shown in Fig. 2b. The technicolor and Z' models are excluded.

8 Summary

In summary, we have studied the invariant mass spectrum m_{jj} of the two jets with the highest transverse momenta in events with two or three jets produced in association with a W boson

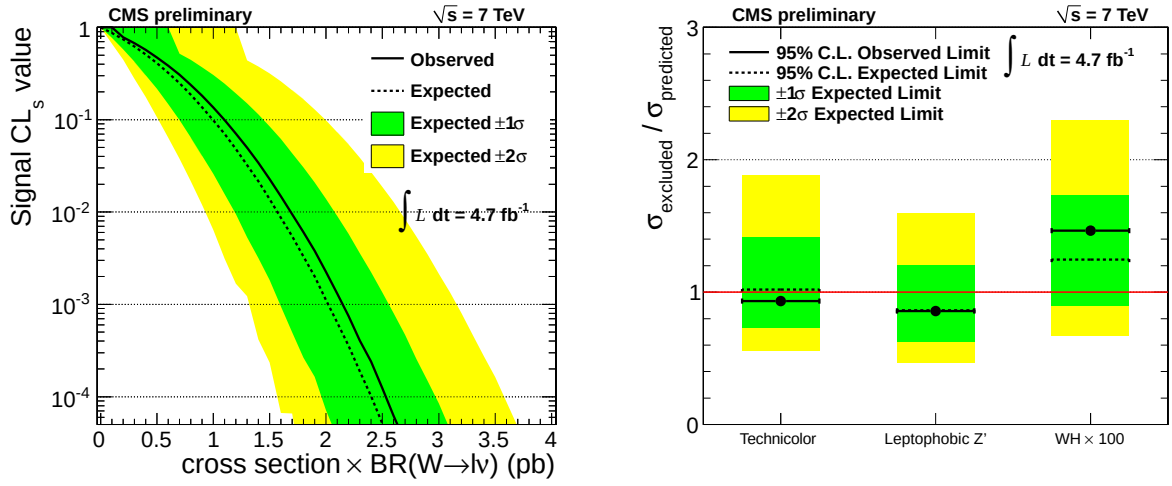

(a) (b)

Figure 2: (a) The observed and expected values of the CL_S statistic for a generic Gaussian signal hypothesis with M=150 GeV, width=15 GeV, as a function of the cross section of the signal times the W$\to \ell\nu$ branching fraction. (b) Observed and expected 95% CL upper limits, with one and two sigma error bands, on the cross section for various signal models. The limits were calculated using the CL_S method. A ratio of the excluded cross section over the predicted cross section smaller than one indicates that the model is excluded at 95% CL. Table 4 lists the cross sections for these models.

that decays leptonically. The analyzed data sample corresponds to an integrated luminosity of 4.7 fb^{-1} collected with the CMS detector at $\sqrt{s} = 7$ TeV in 2010 and 2011. We find no evidence for a resonant enhancement near a dijet mass of 150 GeV. Several theoretical models that predict the presence of a resonant enhancement near 150 GeV are excluded.

References

[1] CDF Collaboration, "Invariant Mass Distribution of Jet Pairs Produced in Association with a W boson in ppbar Collisions at sqrt(s) = 1.96 TeV", *Phys. Rev. Lett.* **106** (2011) 171801, arXiv:1104.0699. doi:10.1103/PhysRevLett.106.171801.

[2] DØ Collaboration, "Bounds on an anomalous dijet resonance in W+jets production in ppbar collisions at sqrts =1.96 TeV", *Phys. Rev. Lett.* **107** (2011) 011804, arXiv:1106.1921.

[3] E. J. Eichten, K. Lane, and A. Martin, "Technicolor at the Tevatron", arXiv:1104.0976.

[4] Adam Martin, private communication.

[5] M. R. Buckley, D. Hooper, J. Kopp et al., "Light Z' Bosons at the Tevatron", *Phys.Rev.* **D83** (2011) 115013, arXiv:1103.6035. doi:10.1103/PhysRevD.83.115013.

[6] Matthew Buckley, private communication.

[7] "The CMS experiment at the CERN LHC", *Journal of Instrumentation* **3** (2008), no. 08, S08004.

[8] CMS Collaboration, "Missing transverse energy performance of the CMS detector", *JINST* **6** (2011), no. 09, P09001, arXiv:1106.5048. doi:10.1088/1748-0221/6/09/P09001.

[9] CMS Collaboration, "Measurement of Inclusive W and Z Cross Sections in pp Collisions at $\sqrt{s} = 7$ TeV", *JHEP* **10** (2011) 132, arXiv:1107.4789v1. doi:10.1007/JHEP10(2011)132.

[10] CMS Collaboration, "Particle–Flow Event Reconstruction in CMS and Performance for Jets, Taus, and $\not\!\!E_{\mathrm{T}}$", *CMS Physics Analysis Summary* **CMS-PAS-PFT-09-001** (2009).

[11] M. Cacciari, G.P. Salam, and G. Soyez, The anti-kt jet clustering algorithm, JHEP 0804, (2008) 063.

[12] M. Cacciari and G.P. Salam,, "Pileup subtraction using jet areas (hep-ph/0707.1378)", *Physics Letters* **B 659** (2008) 119–126. doi:10.1016/j.physletb.2007.09.077.

[13] M. Cacciari, G.P. Salam and G. Soyez, "The catchment area of jets (hep-ph/0802.1188)", *JHEP* **0804** (2008) 005. doi:10.1088/1126-6708/2008/04/005.

[14] CMS Collaboration, "Identification and Filtering of Uncharacteristic Noise in the CMS Hadron Calorimeter", *JINST* **5** (2010) T03014, arXiv:0911.4881. doi:10.1088/1748-0221/5/03/T03014.

[15] CMS Collaboration, "Determination of Jet Energy Calibration and Transverse Momentum Resolution in CMS", *JINST* **6** (2011) P11002, arXiv:1107.4277. doi:10.1088/1748-0221/6/11/P11002.

[16] E. Eichten, K. Lane, and A. Martin, "Testing CDF's Dijet Excess and Technicolor at the LHC", arXiv:1107.4075.

[17] F. Maltoni and T. Stelzer, "MadEvent: Automatic event generation with MadGraph", *JHEP* **02** (2003) 027, arXiv:hep-ex/0208156.

[18] T. Sjostrand, S. Mrenna, and P. Z. Skands, "PYTHIA 6.4 Physics and Manual", *JHEP* **05** (2006) 026, arXiv:hep-ph/0603175.

[19] S. Frixione, P. Nason, and C. Oleari, "Matching NLO QCD computations with parton shower simulations: the POWHEG method", *JHEP* **11** (2007) 070. doi:10.1088/1126-6708/2007/11/070.

[20] CMS Collaboration Collaboration, "Measurement of the Underlying Event Activity at the LHC with $\sqrt{s} = 7$ TeV and Comparison with $\sqrt{s} = 0.9$ TeV", *JHEP* **09** (2011) 109, arXiv:1107.0330. doi:10.1007/JHEP09(2011)109.

[21] H.-L. Lai, J. Huston, Z. Zi et al., "Uncertainty induced by QCD coupling in the CTEQ global analysis of parton distributions", *Phys. Rev. D* **82** (2010) 054021, arXiv:1004.4624. doi:10.1103/PhysRevD.82.054021.

[22] S. Agostinelli et al., GEANT4 Collaboration, "GEANT4: A simulation toolkit", Nucl. Instr. and Methods A 506 (2003) 250-303.

[23] J. Campbell and R.K. Ellis, "Monte Carlo for FeMtobarn processes", http://mcfm.fnal.gov/.

[24] N. Kidonakis, "Next-to-next-to-leading soft-gluon corrections for the top quark cross section and transverse momentum distribution", *Phys. Rev.* **D82** (2010) 114030, arXiv:1009.4935. doi:10.1103/PhysRevD.82.114030.

[25] N. Kidonakis, "NNLL resummation for s-channel single top quark production", *Phys.Rev.* **D81** (2010) 054028, arXiv:1001.5034. doi:10.1103/PhysRevD.81.054028.

[26] N. Kidonakis, "Next-to-next-to-leading-order collinear and soft gluon corrections for t-channel single top quark production", *Phys.Rev.* **D83** (2011) 091503, arXiv:1103.2792. doi:10.1103/PhysRevD.83.091503.

[27] N. Kidonakis, "Two-loop soft anomalous dimensions for single top quark associated production with a W- or H-", *Phys.Rev.* **D82** (2010) 054018, arXiv:1005.4451. doi:10.1103/PhysRevD.82.054018.

[28] CMS Collaboration, "Absolute Calibration of the CMS Luminosity Measurement: Summer 2011 Update", CMS Physics Analysis Summary CMS-PAS-EWK-11-001, (2011).

[29] LHC Higgs Cross Section Working Group, S. Dittmaier, C. Mariotti et al., "Handbook of LHC Higgs Cross Sections: 1. Inclusive Observables", *CERN-2011-002* (CERN, Geneva, 2011) arXiv:1101.0593.

[30] A. Djouadi, J. Kalinowski, and M. Spira, "HDECAY: a program for Higgs boson decays in the Standard Model and its supersymmetric extension", *Computer Physics Communications* **108** (1998), no. 1, 56 – 74. doi:10.1016/S0010-4655(97)00123-9.

[31] Particle Data Group Collaboration, "Review of particle physics", *J. Phys.* **G37** (2010) 075021. doi:10.1088/0954-3899/37/7A/075021.

[32] A. L. Read, "Presentation of search results: the CL s technique", *Journal of Physics G: Nuclear and Particle Physics* **28** (2002), no. 10, 2693.

A Additional plots

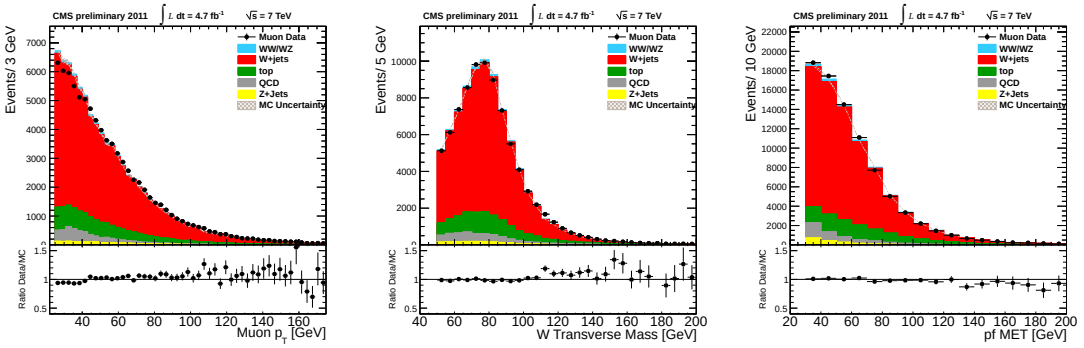

Figure 3: Comparison of the distributions in data and MC for the muon plus jets event sample after event selection (left) of the transverse momentum of the muon candidate, (middle) of the transverse momentum of the reconstructed W candidate, (right) of the missing transverse energy. The error bars on the data points are statistical only. The relative normalization of the various MC samples are taken from the result of the fit to the m_{jj} spectrum.

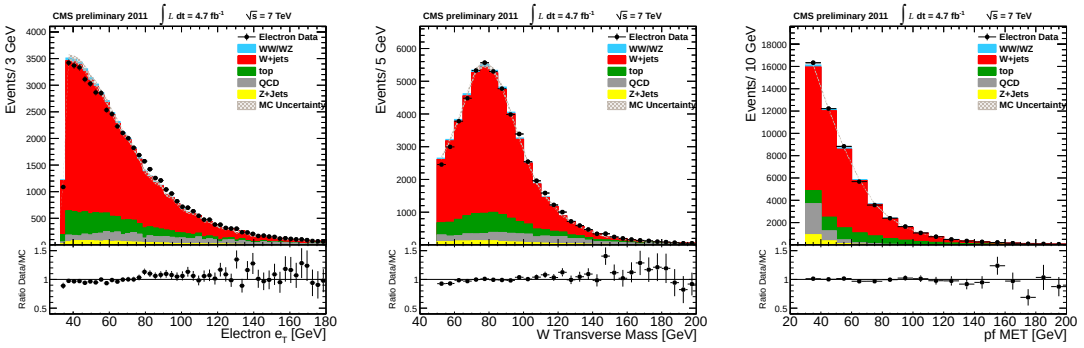

Figure 4: Comparison of the distributions in data and MC for the electron plus jets event sample after event selection (left) of the transverse energy of the electron candidate, (middle) of the transverse momentum of the reconstructed W candidate, (right) of the missing transverse energy. The error bars on the data points are statistical only. The relative normalization of the various MC samples are taken from the result of the fit to the m_{jj} spectrum.

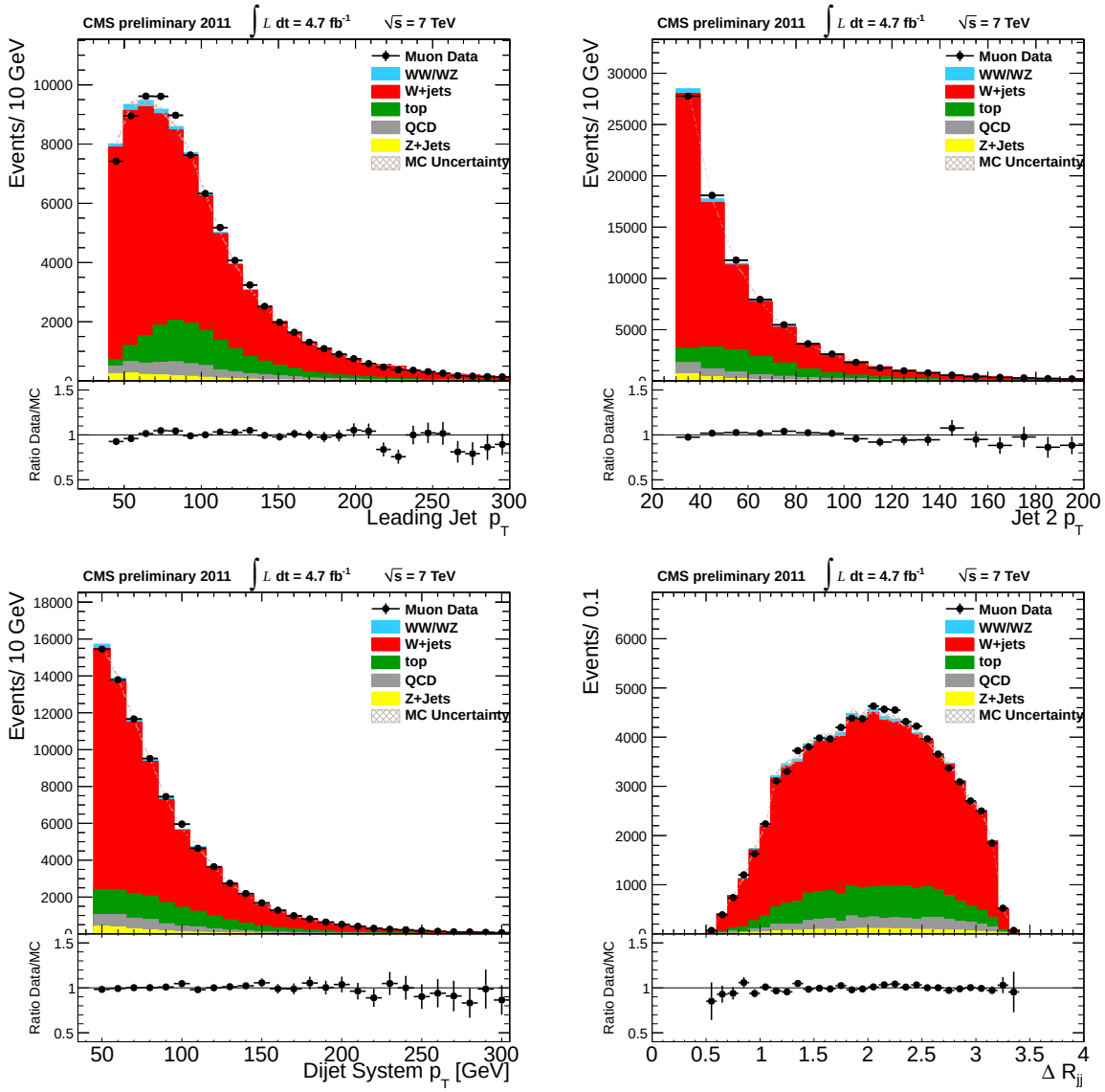

Figure 5: Comparison of the distributions in data and MC for the muon plus jets event sample after event selection (upper left) of the transverse momentum of the leading jet, (upper right) of the transverse momentum of the second leading jet, (lower left) of the dijet transverse momentum, (lower right) of the dijet distance parameter $\Delta R = \sqrt{(\Delta\eta_{jj})^2 + (\Delta\phi_{jj})^2}$. The error bars on the data points are statistical only. The relative normalization of the various MC samples are taken from the result of the fit to the m_{jj} spectrum.

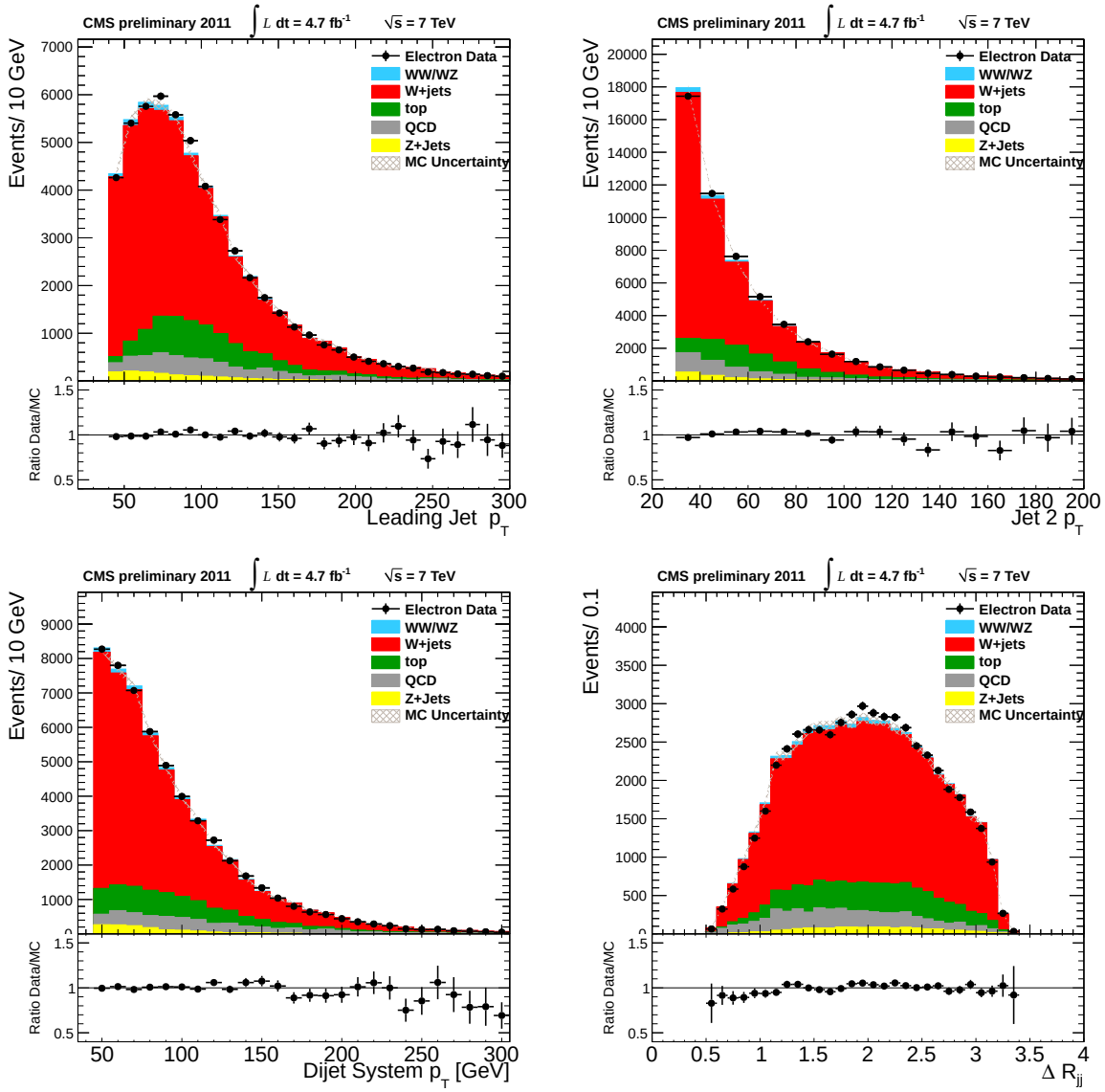

Figure 6: Comparison of the distributions in data and MC for the electron plus jets event sample after event selection (upper left) of the transverse momentum of the leading jet, (upper right) of the transverse momentum of the second leading jet, (lower left) of the dijet transverse momentum, (lower right) of the dijet distance parameter $\Delta R = \sqrt{(\Delta\eta_{jj})^2 + (\Delta\phi_{jj})^2}$. The error bars on the data points are statistical only. The relative normalization of the various MC samples are taken from the result of the fit to the m_{jj} spectrum.